



Cite this: *Mater. Adv.*, 2024,
5, 3992

Al₂O₃ growth in PMMA thin films by sequential infiltration synthesis: *in situ* thickness evolution and mass uptake investigation

Michele Perego,  * Gabriele Seguíni,  * Claudia Wiemer, Federica E. Caligiore and Elena Cianci

Sequential infiltration synthesis (SIS) represents a simple and straightforward approach to grow inorganic materials in polymeric films. In this work a combination of *in situ* and *ex situ* spectroscopic ellipsometry (SE) analysis is used to provide a comprehensive picture of polymer film evolution and Al₂O₃ incorporation as a function of the number of SIS cycles. Two different growth regimes can be clearly distinguished. Initially, Al₂O₃ incorporation determines a marked swelling of polymer films during each SIS cycle. Subsequently, no significant variation of the polymer film thickness is observed by means of *in situ* SE, despite Al₂O₃ mass uptake at each SIS cycle being clearly highlighted by the gradual increase of the refractive index observed by *in situ* SE as well as by the regular increment of Al₂O₃ film thickness detected by *ex situ* SE. The experimental data suggest that after a few SIS cycles, Al₂O₃ growth in the polymer film results in a rigid inorganic–organic template. Precursor penetration determines further incorporation of Al₂O₃ within its volume during subsequent SIS cycles, without any significant swelling of the template. This picture is supported by *ex situ* X-ray reflectivity (XRR) analysis of the infiltrated polymer films and the residual Al₂O₃ film upon removal of the organic matrix.

Received 21st December 2023,
Accepted 10th March 2024

DOI: 10.1039/d3ma01159c

rsc.li/materials-advances

Introduction

Sequential infiltration synthesis (SIS), also referred to as vapor phase infiltration (VPI), provides a successful route to grow inorganic materials in polymeric films by the penetration of gaseous precursors into the polymer,^{1–3} in order to enhance the functional properties of the polymer creating an organic–inorganic hybrid material^{4–9} or to fabricate inorganic nanostructures when infiltrating in patterned polymer films.^{10–14} In particular, SIS has been proposed as a powerful tool to generate inorganic nanostructures starting from self-assembled block copolymer templates. Depending on the specific morphology of the block copolymer template different inorganic nanostructures can be obtained, providing a simple and cost-effective tool to generate periodic inorganic nanostructures over large areas.^{15–18} A theoretical framework for the description of this process has been outlined in a couple of seminal papers by Leng and Loege,^{7,19} providing a first indication of the different phenomena taking place during a SIS process. However, several fundamental aspects of the SIS process are not fully understood yet.^{20–25} More experimental work is necessary to better elucidate the physico-chemical phenomena taking

place during SIS and to validate the theoretical description of the process, developing predictive models²⁶ that can help to enlarge the number of materials^{27,28} grown by SIS and speed up the exploitation of this technology at the industrial level.

In this work Al₂O₃ mass uptake into poly(methyl methacrylate) (PMMA) thin films is investigated by means of a combination of *in situ* and *ex situ* characterization techniques, achieving information about the evolution of the polymer template during the Al₂O₃ incorporation.

Experimental

Sample preparation and cleaning

The 1 × 1 cm² Si substrates were cleaned using piranha solution (H₂SO₄:H₂O₂ = 3:1 vol. ratio) at 80 °C for 40 min, rinsed with 2-propanol in an ultrasonic bath and finally dried in N₂ flux. PMMA (*M*_n = 14 kg mol^{−1}, PDI 1.2) was dissolved in toluene before casting, properly adjusting the concentration to obtain polymer films with the desired thickness (*H*). Before infiltration, the films were thermally annealed at 250 °C for 900 s in a N₂ atmosphere by means of a Rapid Thermal Process (RTP) tool (Jipelec Jetfirst 100) in order to remove residual toluene from the polymer films.

IMM-CNR Agrate Unit, Via C. Olivetti 2, Agrate Brianza I-20864, Italy.
E-mail: michele.perego@cnr.it, gabriele.seguini@cnr.it



Sequential infiltration synthesis

Samples were loaded in a Savannah 200 Ultratech Cambridge NanoTech cross flow ALD reactor and thermalized at 90 °C for 30 min under 100 sccm N₂ flow at 0.6 Torr before starting the infiltration. Al₂O₃ SIS used alternated exposure to TMA (Aldrich, 97%) and deionized H₂O intercalating to a purge phase in N₂ flow at 100 sccm. In particular, each TMA half-cycle was composed of a TMA pulse ($t = 0.025$ s) followed by a 60 s exposure step and a 60 s purge step. Similarly, the H₂O half-cycle was made by a H₂O pulse ($t = 0.015$ s) followed by a 60 s long exposure step and a 180 s long purge step. More details of the SIS cycle process are reported in a previous publication.^{6,29,30} During the SIS process, thin film samples were exposed to O₂ plasma to remove the polymer matrix, resulting in the formation of Al₂O₃ films on the silicon substrate. Finally, the samples were annealed at 900 °C for 60 s in a N₂ atmosphere using a conventional RTP system.

Ellipsometry analysis

The ellipsometric data were collected using a rotating compensator ellipsometer equipped with a Xe lamp (M-2000F, J. A. Woollam Co. Inc.) in the wavelength range of 250–1000 nm at a fixed incidence angle of 75°. The ellipsometric data were analyzed using the EASE software package 2.3 version (J. A. Woollam Co. Inc.). Two quartz windows installed on the ALD reactor lid allowed performing the *in situ* characterization of the polymer film during the SIS process.²⁹ To estimate the polymer layer thickness, ellipsometric data were fitted using a film stack model composed of a Cauchy model on SiO₂ on the silicon substrate in the wavelength range of 400–1000 nm, because of the absorbing nature of the ester group in the ultraviolet range. The silicon dioxide thickness was previously acquired before spin casting for each sample to better fit the Cauchy model after the spin process. The *in situ* SE data were fitted using both a Cauchy model and an effective medium approximation (EMA) model.

XRR analysis

X-ray reflectivity (XRR) analysis was performed with a Italstruc-tures HRXRD2000 system, equipped with a Cu K_α sealed tube, a four circle goniometer and a scintillator detector. XRR patterns were simulated using a model based on the matrix formalism corrected by a Croce–Nevot factor. The layer thickness, surface and interfacial roughness and density of each layer were retrieved from the fitting of the experimental data.

Results and discussion

In situ spectroscopic ellipsometry (SE) is an extremely powerful method for the real-time monitoring of the SIS process. Time resolution of the spectroscopic ellipsometry guarantees acquisition of information about *intra-cycle* sample evolution as demonstrated by Cianci *et al.* in a previous work.²⁹ In particular, swelling and deswelling during each SIS cycle were associated with sorption and desorption of TMA and H₂O

molecules. Moreover, swelling curves were demonstrated to directly correlate with mass uptake into the PMMA films, providing the possibility to determine the diffusion coefficient of TMA in the polymer matrix.²⁹ In addition, SE analysis offers the possibility of *in situ* monitoring the thickness (H) and refractive index (n) evolution during the whole SIS process, obtaining information about the characteristic of the polymer film during each SIS cycle.

Fig. 1a and b show the evolution of H and n for a 55 nm thick PMMA film during the 10 cycle SIS process performed at 90 °C using TMA and H₂O. H and n values were obtained by fitting the SE data with the standard Cauchy model. The values of the total

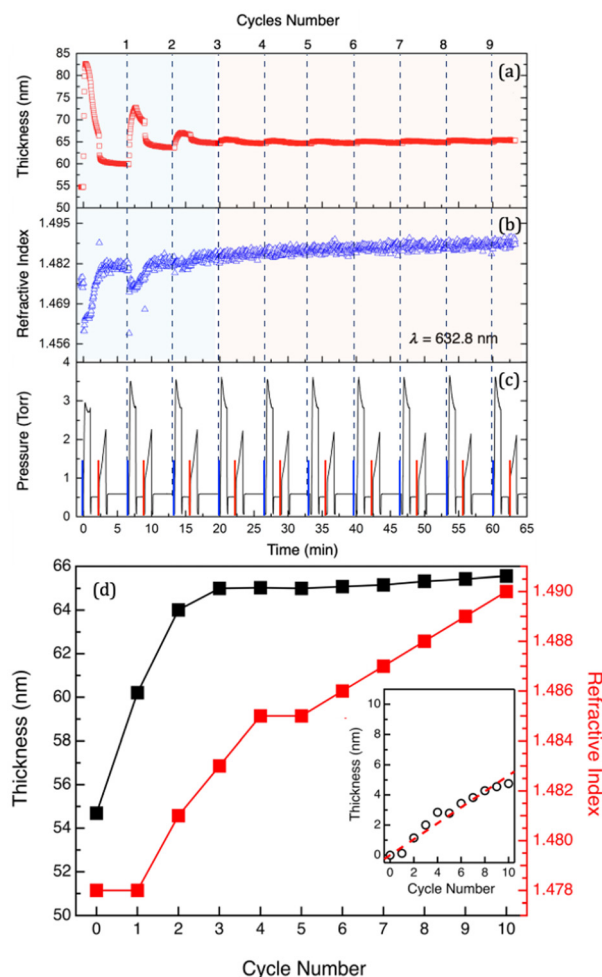


Fig. 1 (a) Thickness, (b) refractive index of the 55 nm thick PMMA film and (c) pressure in the main chamber during the 10 cycle SIS process performed at 90 °C using TMA and H₂O as metal and oxygen precursors, respectively. TMA and H₂O injection into the chamber are indicated by blue and red lines, respectively. Data are reported as a function of the processing time. (d) Thickness and refractive index values at the end of each SIS cycle. Values were obtained from the average of the thickness and refractive index extracted from the *in situ* spectroscopic ellipsometry data during the final purge in N₂ at the end of each cycle. The inset reports the equivalent Al₂O₃ thickness, *i.e.* the thickness of an Al₂O₃ film with the same volume of the Al₂O₃ fraction that is present in the infiltrated sample according to the fitting of the ellipsometry data by means of an effective medium approximation model.

pressure within the growth chamber are reported in Fig. 1c to highlight the different steps of the SIS process. The pressure variations over the different steps of each cycle are systematically reproduced cycle after cycle apart from the pressure during the TMA exposure step of the first cycle. The lower pressure in the chamber during TMA exposure in the first cycles compared to the following ones is tentatively attributed to a larger amount of TMA incorporated in the PMMA matrix during the first cycle, resulting in a reduction of the TMA partial pressure in the chamber. Interestingly, in each cycle, a significant and systematic pressure decrease/increase is observed during TMA/H₂O exposure. Since during exposure steps the chamber is in a static vacuum, the pressure reduction during TMA exposure is tentatively attributed to a reduction of the TMA partial pressure in the chamber due to the reaction of the TMA molecules with water vapor released from the walls of the growth chamber. A pressure reduction due to sorption of molecules in the PMMA film can be ruled out considering the small size of the samples. In addition, the same pressure reduction is observed when operating the system without loading any sample into the chamber further supporting our previous hypothesis. Conversely, the release of H₂O molecules from the chamber walls is expected to determine a pressure increase during H₂O exposure. Additionally, we could speculate about the role of the reaction byproducts (CH₄) generated by the reaction of H₂O with TMA molecules chemisorbed in the polymer film or on the wall chamber. Nevertheless, we have to consider that this reaction is very fast. Consequently, we would expect this phenomenon to induce a very fast pressure increase in the chamber and not a progressive variation as shown in Fig. 1c.

Data in Fig. 1a and b clearly indicate the occurrence of two different regimes during the Al₂O₃ infiltration process. In the first cycle, the film thickness largely increases during TMA injection and exposure and subsequently decreases during the following TMA purge and H₂O exposure. During the second and third cycles, the sample still exhibits large thickness changes during TMA injection and exposure steps although the absolute values of the thickness increase are smaller than that obtained during the first SIS cycle for pristine PMMA. Starting from the fourth cycle on, a very small thickness variation is observed during each TMA exposure step. The values of the film thickness (H_n) and refractive index n_n at the end of the n th SIS cycle are reported in Fig. 1d. Interestingly, H_n rapidly increases over the first 3–4 cycles and subsequently levels off achieving an almost constant H_n value. This level-off is usually considered as a signature of the fact that no Al₂O₃ infiltration occurs upon the first 3–4 cycles, because of the formation of an Al₂O₃ film on top of the hybrid organic–inorganic matrix. In this picture, the very limited thickness increase of the film after the first 3–4 cycles is associated with an ALD-like growth on the surface of the film.²⁹ Actually, the appropriate interpretation of these experimental data requires to take into account the evolution of n_n , that is progressively increasing cycle after cycle, as shown in Fig. 1d. This evolution of the n_n values suggests that incorporation of Al₂O₃ into the

PMMA matrix takes place even after the first 3–4 cycles. Accordingly, by fitting the data using an EMA model, it is possible to correlate the refractive index evolution with a progressive increase of the Al₂O₃ fraction incorporated into the PMMA film.

This model assumes the presence, in the volume of the film, of two components corresponding to PMMA and Al₂O₃, respectively. Interestingly, the model returns film thickness values that are perfectly equivalent to the ones obtained using a simple Cauchy model, within the experimental error. In addition, as a result of this fitting procedure, the EMA model provides the volume fraction of Al₂O₃ that is present in the infiltrated polymer film. Accordingly, it is possible to calculate the volume of Al₂O₃ that has been incorporated into the polymer film at each cycle. The inset of Fig. 1d reports the evolution, as a function of the number of SIS cycles, of the equivalent Al₂O₃ thickness, *i.e.* the thickness of an Al₂O₃ film with the same volume of the Al₂O₃ fraction that is present in the infiltrated sample according to the fitting of the ellipsometry data. By fitting the experimental data (dashed line), the growth rate of the Al₂O₃ film was determined to be $0.53 \text{ nm} \pm 0.02 \text{ nm cycle}^{-1}$. It is worth noting that, for the fitting of the SE data, the system is assumed to be composed of two distinct phases having the refractive index of the pristine PMMA ($n_{\text{PMMA}} = 1.478$) at 90 °C and of a 17.5 nm thick Al₂O₃ film ($n_{\text{Al}_2\text{O}_3} = 1.625$) grown by ALD at 90 °C, respectively. This assumption returns an oversimplified model of the system, making the estimation of the Al₂O₃ fraction incorporated into the PMMA film questionable in terms of absolute values. Nevertheless, this analysis of the experimental data supports the idea that Al₂O₃ incorporation goes on even if no further swelling of the PMMA film is detected at the end of the SIS cycle. In addition, it is worth to note that the *ex situ* analysis of the same sample upon 10 SIS cycles returned a film thickness of $H = 68.8 \pm 0.1 \text{ nm}$ and a refractive index of $n = 1.511 \pm 0.005$. These values are significantly larger than the ones obtained by *in situ* measurements at the end of the SIS process, suggesting that further evolution of the sample occurred upon exposure to air.

In order to clarify all these points, *ex situ* analyses of infiltrated PMMA films, before and after removal of the organic phase by O₂ plasma, were performed as a function of the number of SIS cycles. In particular, PMMA samples were prepared by spin coating and subsequently infiltrated with different numbers of SIS cycles. The thickness of the PMMA films was adjusted in order to guarantee complete infiltration of the polymer film using TMA at 90 °C according to the diffusivity coefficient values determined by *in situ* investigation in a previous work.^{29,30} The average thickness of the pristine PMMA films was determined to be $H_{\text{PMMA}} = 44.6 \pm 0.7 \text{ nm}$ as shown in Fig. 2a. The limited dispersion of the initial thickness values guarantees that measured variations of the mass uptake values do not depend on the volume of the infiltrated PMMA matrix. Fig. 2a and b show the evolution of the polymer film thickness and refractive index as a function of the number of SIS cycles. The *ex situ* measurements of the PMMA films upon



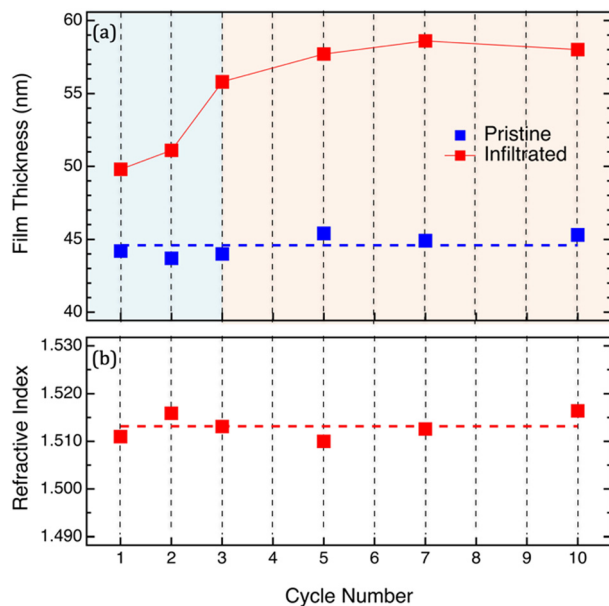


Fig. 2 (a) Thickness of pristine PMMA films (blue symbols) and the same sample upon infiltration of Al_2O_3 at 90°C (red symbols). Thickness values are reported as a function of the number of SIS cycles performed on each sample. The thickness of the infiltrated PMMA samples was measured *ex situ* upon exposure to air. The dashed line indicates the average thickness value of the pristine PMMA films. (b) Refractive index of the infiltrated samples reported as a function of the number of SIS cycles. The thickness and refractive index values were obtained by the fitting of SE data using a standard Cauchy model. The dashed line indicates the average refractive index value of the infiltrated samples.

infiltration confirmed the trend already observed during the *in situ* analysis: film thickness progressively increases as a function of the number of SIS cycles during the initial stages of the process and subsequently levels-off achieving a steady state value corresponding to $H = 58 \pm 1$ nm. Interestingly, according to *ex situ* measurements, the refractive index of the infiltrated sample is fairly constant with an average value of $n = 1.513 \pm 0.002$. We assume that this almost constant n value irrespective of the number of SIS cycles is a consequence of the modification of the samples occurring during exposure to air and consequent moisture absorption in the infiltrated PMMA film. Accordingly, we can speculate that the incorporation of water into the infiltrated sample when exposed to air significantly modifies the oxidation state of the infiltrated aluminum component. *In situ* chemical analysis of the Al bonding configuration would be necessary to support this hypothesis. Moreover, the comparison between *in situ* and *ex situ* measurements suggests that any modelling of the effective evolution of the sample during the process on the basis of *ex situ* analysis of the samples has to be critically evaluated.

Upon the removal of the PMMA phase by O_2 plasma treatment, the samples were analyzed by SE and XRR to obtain information about the residual amount of Al_2O_3 that is left over the substrate. Fig. 3a shows the thickness values of the Al_2O_3 film measured by SE (black closed symbols) showing a linear increase of the film as a function of the number of SIS cycles.

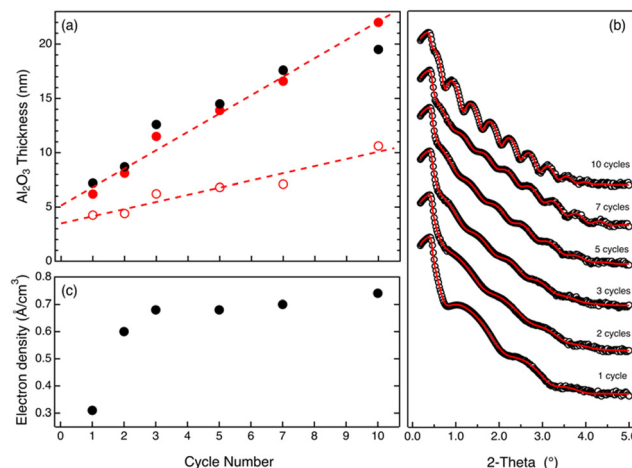


Fig. 3 (a) Thickness of the Al_2O_3 films obtained upon infiltration into 45 nm thick PMMA films and subsequent removal of the organic phase by O_2 plasma. The thickness values were obtained by SE (red closed symbols) and XRR (black closed symbols) analyses of the same set of samples. The thickness values are reported as a function of the number of SIS cycles performed on each sample. The thickness values (red open symbols) of the same Al_2O_3 films upon annealing in a N_2 atmosphere at 900°C for 60 s are reported as well. The dashed lines correspond to linear fittings of the experimental data. (b) XRR spectra of the Al_2O_3 film upon infiltration into 45 nm thick PMMA films and subsequent removal of the organic phase by O_2 plasma. The solid lines correspond to fitting of the experimental data. (c) Electron density of the Al_2O_3 films reported as a function of the number of SIS cycles.

The data clearly highlight a linear increase of the film thickness cycle after cycle, confirming that the incorporation of Al_2O_3 continues even when no swelling of the polymer film is detected during *in situ* SE analysis. According to the experimental data, the Al_2O_3 film thickness is below 10 nm for some of the samples. In this thickness regime, the thickness and refractive index cannot be considered as independent variables anymore. In this case, a simple fitting of the experimental data using a Cauchy model returns proper evaluation of the film thickness, but refractive index values do not provide any reliable information about the density of Al_2O_3 . Fig. 3b shows the XRR spectra for the same samples. From the fitting (solid lines) of the experimental data (open symbols), the thickness and electronic density of each sample were determined. The thickness values (red closed symbols) obtained by the analysis of the XRR spectra are reported in Fig. 3a. These values are in excellent agreement with those obtained by SE measurements, confirming the progressive increase of the Al_2O_3 film thickness over the 10 cycle SIS process. Fig. 3c reports the values of electronic density as a function of the number of SIS cycles for each sample. The electronic density increases over the first 3 cycles achieving a saturation value of $0.7 \text{ e } \text{\AA}^{-3}$.

Actually, electronic density values determined by analysis of XRR data indicate that, after the first 3 SIS cycles, the density of the Al_2O_3 films is around $2.3 \times 10^{-12} \text{ ng nm}^{-3}$. This value is significantly lower than the one obtained in the case of samples grown by a standard ALD process at 90°C that is usually reported to be $2.7 \times 10^{-12} \text{ ng nm}^{-3}$.³¹ An additional thermal



treatment in a N₂ atmosphere at 900 °C for 60 s was performed to promote Al₂O₃ densification, determining a significant shrinking of the Al₂O₃ films. Fig. 3a reports the thicknesses (black open symbols) of the densified Al₂O₃ films as a function of the number of SIS cycles. Data indicate a progressive increase of the Al₂O₃ film thickness. According to the linear fitting (dashed line) of the experimental data, the growth per cycle is determined to be 0.66 nm ± 0.09 nm cycle⁻¹. This value is fairly consistent, within the experimental error, with the one obtained by *in situ* SE analysis. Moreover, the growth per cycle value obtained by this analysis is significantly higher than the one obtained by standard ALD at 90 °C that is reported to be around 0.1 nm cycle⁻¹.^{11,31}

All these data further corroborate our interpretation of the *in situ* SE data and demonstrate that the SIS process takes place even when no swelling of the polymer film is detected, ruling out the hypothesis of an Al₂O₃ growth on the surface of the organic–inorganic film *via* an ALD-like process. Accordingly, we assume that after a few SIS cycles, Al₂O₃ growth in the polymer film results in the formation of a rigid inorganic–organic template due to the formation of a Al₂O₃ network interpenetrated with the polymer matrix. The porosity of this hybrid material is high enough to enable diffusion of precursor molecules into the film and, consequently, Al₂O₃ growth into the volume. Nevertheless, we expect that the free volume of this rigid inorganic–organic template is much lower than the one of the swollen polymer matrix during the first cycle. Accordingly, a limited amount of TMA molecules is expected to penetrate into the film compared to the first cycle, which is characterized by an extremely large swelling of the polymer matrix during TMA exposure. This could account for the very large increase of the Al₂O₃ film thickness that is observed during the first cycle, determining the formation of a 4.3 ± 0.1 nm thick Al₂O₃ film. Conversely, as shown in Fig. 3a, upon the first cycle, an almost linear increase of the Al₂O₃ film thickness with a constant growth rate of 0.66 nm ± 0.09 nm cycle⁻¹ is observed, suggesting that being irrespective of the specific swelling evolution, the same amount of Al₂O₃ is incorporated into the film during each SIS cycle. Furthermore, this result clearly highlights the specificity of the first cycle, suggesting that any theory for the modelling of the SIS process has to take into account swelling of the polymer matrix and progressive evolution of the properties of the polymer due to Al₂O₃ incorporation cycle after cycle.

From a general perspective, during SIS, several chemico-physical processes take place at the same time, generating a dynamic equilibrium that changes at each step of the process. Infiltration of TMA into PMMA represents a quite peculiar system because the reactivity of TMA with PMMA is quite slow, irrespective of the processing temperature. In a recent paper Weisbord *et al.* demonstrated that the maximum mass gain for TMA in PMMA is expected to occur at a processing temperature $T \sim 70$ °C.²¹ At higher temperatures the reactivity is progressively reduced resulting in a low mass uptake. In this respect, operating at 70 °C appears to be the best choice to maximize the stable incorporation of TMA molecules into the PMMA matrix. Nevertheless, even performing the process at $T = 70$ °C, the

reactivity is not high enough to guarantee the complete saturation of the reactive sites in the PMMA matrix. Additionally, we have to consider that a reduction of the processing temperature implies a reduction of TMA diffusivity, limiting the capability to effectively infiltrate thick PMMA films. In this respect, the choice to perform the experiment at 90 °C represents a compromise in order to guarantee full infiltration of the 50 nm thick polymer film achieving a high Al₂O₃ mass uptake over the 10 SIS cycles.²⁹

In agreement with this picture, significant out-diffusion of the unreacted TMA molecules is observed to occur during the purging step.²⁹ This is clearly highlighted in Fig. 1a by the significant deswelling of the PMMA film during purging in N₂. Actually, this phenomenon has been widely discussed in the literature and it has to be considered as an intrinsic characteristic of this specific precursor–polymer combination. In particular, Petit *et al.* showed that TMA out-diffusion during purging is significantly enhanced at 125 °C, resulting in an almost complete desorption of the TMA molecules.²² This experimental result is perfectly consistent with the idea that reactivity is progressively reduced by increasing the processing temperature, reducing the effective capability to infiltrate Al₂O₃ in the polymer template. Accordingly, irrespective of the duration of the purging process, the unreacted TMA molecules are expected to play a role in the growth of Al₂O₃ into the PMMA matrix. The reaction of H₂O with the residual TMA vapor into the PMMA matrix determines the formation of Al₂O₃ seeds that provides additional reactive sites for TMA during the subsequent SIS cycles: the higher the number of Al₂O₃ seeds that are formed in the polymer matrix upon each cycle, the faster is expected to be the formation of an Al₂O₃ network in the polymer matrix. In this respect, the presence of this unreacted TMA molecule into the PMMA film does not change the overall picture: after a certain amount of SIS cycles, a rigid inorganic–organic template is formed preventing swelling/deswelling of the polymer matrix during the SIS cycles.

In particular, as shown in a previous paper,²⁹ even in the case of a very long purge time ($t = 500$ s), the formation of Al₂O₃ seeds into the PMMA matrix is observed after only a single SIS cycle. Additionally, in a more recent paper,³⁰ a direct correlation between mass uptake and the concentration of reactive sites in the polymer matrix was highlighted during the SIS process at $T = 90$ °C, suggesting that a significant contribution to infiltration of Al₂O₃ into the PMMA film comes from the reacted TMA molecules. Moreover, TMA infiltration in PS thin films, where no reactive sites are present, results in a very limited incorporation of Al₂O₃ in the polymer film.³⁰

Conclusions

In situ and *ex situ* spectroscopic ellipsometry analyses were combined to understand the kinetics of Al₂O₃ incorporation into PMMA during a SIS process performed at 90 °C using TMA and H₂O as metal and oxygen precursors, respectively. *Ex situ* XRR measurements were performed for the infiltrated samples



before and after O₂ plasma treatment for the removal of the organic phase. XRR results were compared with those obtained by SE in order to provide a comprehensive picture of the system evolution. The collected data indicate a progressive incorporation of Al₂O₃ cycle after cycle with a constant mass uptake. Interestingly the initial SIS cycles are characterized by significant swelling/deswelling of the polymer film. Conversely, after a few SIS cycles no more swelling of the polymer film is observed, suggesting that Al₂O₃ incorporation into the volume of the polymer film results in the formation of a rigid inorganic-organic structure. Precursor penetration determines further incorporation of Al₂O₃ within the volume of this hybrid material during subsequent SIS cycles, without any significant swelling of the film. Significant modification of the samples is observed to occur upon exposure to air due to moisture or oxygen penetration and incorporation into the inorganic-organic template.

Conflicts of interest

There are no conflicts to declare.

Acknowledgements

This research was partially supported by the project “IONS4-SET” funded from the European Union’s Horizon 2020 research and innovation program (Grant No. 688072).

References

- 1 E. C. Dandley, C. D. Needham, P. S. Williams, A. H. Brozena, C. J. Oldham and G. N. Parsons, *J. Mater. Chem. C*, 2014, **2**, 9416–9424.
- 2 R. P. Padbury and J. S. Jur, *J. Vac. Sci. Technol. Vac. Surf. Films*, 2014, **32**, 041602.
- 3 R. P. Padbury and J. S. Jur, *Langmuir*, 2014, **30**, 9228–9238.
- 4 F. Yang, J. Brede, H. Ablat, M. Abadia, L. Zhang, C. Rogero, S. D. Elliott and M. Knez, *Adv. Mater. Interfaces*, 2017, **4**, 1700237.
- 5 M. Biswas, J. A. Libera, S. B. Darling and J. W. Elam, *ACS Appl. Polym. Mater.*, 2020, **2**, 5501–5510.
- 6 A. Motta, G. Seguíni, M. Perego, R. Consonni, A. C. Boccia, G. Ambrosio, C. Baratto, P. Cerruti, M. Lavorgna, S. Tagliabue and C. Wiemer, *ACS Appl. Polym. Mater.*, 2022, **4**, 17191–7203.
- 7 C. Z. Leng and M. D. Losego, *Mater. Horiz.*, 2017, **4**, 747–771.
- 8 M. Ko, H.-U. Kim and N. Jeon, *ACS Appl. Polym. Mater.*, 2023, **5**, 50–56.
- 9 O. Yurkevich, E. Modin, I. Šarić Janković, R. Peter, M. Petravić and M. Knez, *Chem. Mater.*, 2023, **35**, 7529–7541.
- 10 Q. Peng, Y. Tseng, S. B. Darling and J. W. Elam, *Adv. Mater.*, 2010, **22**, 5129–5133.
- 11 E. C. Dandley, P. C. Lemaire, Z. Zhu, A. Yoon, L. Sheet and G. N. Parsons, *Adv. Mater. Interfaces*, 2016, **3**, 1500431.
- 12 M. Baryshnikova, D. De Simone, W. Knaepen, K. Kachel, B. Chan, S. Paolillo, J. Willem Maes, D. De Roest, P. Rincon Delgadillo and G. Vandenberghe, *J. Photopolym. Sci. Technol.*, 2017, **30**, 667–670.
- 13 N. Tiwale, A. Subramanian, K. Kisslinger, M. Lu, J. Kim, A. Stein and C.-Y. Nam, *J. Mater. Chem. C*, 2019, **7**, 8803–8812.
- 14 A. Subramanian, N. Tiwale, W. Lee, K. Kisslinger, M. Lu, A. Stein, J. Kim and C. Nam, *Adv. Mater. Interfaces*, 2023, **10**, 2300420.
- 15 J. Frascaroli, E. Cianci, S. Spiga, G. Seguíni and M. Perego, *ACS Appl. Mater. Interfaces*, 2016, **8**, 33933–33942.
- 16 C. Zhou, T. Segal-Peretz, M. E. Oruc, H. S. Suh, G. Wu and P. F. Nealey, *Adv. Funct. Mater.*, 2017, **27**, 1701756.
- 17 A. Löfstrand, R. Jafari Jam, K. Mothander, T. Nylander, M. Mumtaz, A. Vorobiev, W.-C. Chen, R. Borsali and I. Maximov, *ACS Appl. Nano Mater.*, 2021, **4**, 5141–5151.
- 18 G. Seguíni, A. Motta, M. Bigatti, F. E. Caligiore, G. Rademaker, A. Gharbi, R. Tiron, G. Tallarida, M. Perego and E. Cianci, *ACS Appl. Nano Mater.*, 2022, **5**, 9818–9828.
- 19 C. Z. Leng and M. D. Losego, *Phys. Chem. Chem. Phys.*, 2018, **20**, 21506–21514.
- 20 R. Z. Waldman, D. J. Mandia, A. Yanguas-Gil, A. B. F. Martinson, J. W. Elam and S. B. Darling, *J. Chem. Phys.*, 2019, **151**, 190901.
- 21 I. Weisbord, N. Shomrat, R. Azoulay, A. Kaushansky and T. Segal-Peretz, *Chem. Mater.*, 2020, **32**, 4499–4508.
- 22 R. R. Petit, J. Li, B. Van De Voorde, S. Van Vlierberghe, P. F. Smet and C. Detavernier, *ACS Appl. Mater. Interfaces*, 2021, **13**, 46151–46163.
- 23 M. Snelgrove, C. McFeely, K. Shiel, G. Hughes, P. Yadav, C. Weiland, J. C. Woicik, P. G. Mani-Gonzalez, R. Lundy, M. A. Morris, E. McGlynn and R. O'Connor, *Mater. Adv.*, 2021, **2**, 769–781.
- 24 J. Ham, M. Ko, B. Choi, H.-U. Kim and N. Jeon, *Sensors*, 2022, **22**, 6132.
- 25 Y. Liu, E. K. McGuinness, B. C. Jean, Y. Li, Y. Ren, B. G. D. Rio, R. P. Lively, M. D. Losego and R. Ramprasad, *J. Phys. Chem. B*, 2022, **126**, 5920–5930.
- 26 Y. Ren, E. K. McGuinness, C. Huang, V. R. Joseph, R. P. Lively and M. D. Losego, *Chem. Mater.*, 2021, **33**, 5210–5222.
- 27 R. Z. Waldman, N. Jeon, D. J. Mandia, O. Heinonen, S. B. Darling and A. B. F. Martinson, *Chem. Mater.*, 2019, **31**, 5274–5285.
- 28 N. Poonkottil, E. Solano, A. Muriqi, M. M. Minjauw, M. Filez, M. Nolan, C. Detavernier and J. Dendooven, *Chem. Mater.*, 2022, **34**, 10347–10360.
- 29 E. Cianci, D. Nazzari, G. Seguíni and M. Perego, *Adv. Mater. Interfaces*, 2018, **5**, 1801016.
- 30 F. E. Caligiore, D. Nazzari, E. Cianci, K. Sparnacci, M. Laus, M. Perego and G. Seguíni, *Adv. Mater. Interfaces*, 2019, **6**, 1900503.
- 31 M. D. Groner, F. H. Fabreguette, J. W. Elam and S. M. George, *Chem. Mater.*, 2004, **16**, 639–645.

